

Advanced Real-Time Synchronphasor Applications

Edmund O. Schweitzer, III, David Whitehead, Armando Guzman, Yanfeng Gong, and Marcos Donolo, *Schweitzer Engineering Laboratories, Inc.*

Abstract—Advances in synchronphasor technology have led to synchronphasor applications progressing from being simply visualization, data archiving, and postmortem analysis tools to real-time control systems. These new systems can produce, consume, time align, and process synchronphasor data. A significant advancement in this technology is that the results of synchronphasor processing translate into alarm or control actions that are issued in real time. With this powerful, new technology, former complex synchronphasor applications such as system integrity protection schemes (SIPS) and assessment of power system stability over large geographical areas are easier to implement, have fewer components, and are more reliable than traditional solutions. The paper discusses how to accomplish the following tasks:

- Detecting out-of-step conditions.
- Identifying inter-area power oscillations.
- Protecting multi-terminal substation busbars.
- Identifying current and voltage measurement errors.

I. INTRODUCTION

The Synchronphasor Vector Processor (SVP) [1] and relays can simplify and improve SIPSs that use synchronphasors. Fig. 1 shows Bonneville Power Administration's SIPS that uses synchronphasors [2]. This system under evaluation consists of Phasor Measurement Units (PMUs), a Phasor Data Concentrator (PDC), a Wide-Area Control System (WACS) controller, and a Wide-Area Protection System (WAPS) controller.

The SVP performs the PDC, WACS, and WAPS functions of the system shown in Fig. 1. It receives synchronphasors, analog quantities, and binary inputs from remote relays, correlates the received data, and processes protection and control algorithms deterministically. Additionally, the SVP uses GOOSE [3], Fast Message [4], and MIRRORED BITS[®] communications [5] protocols to activate commands based on the processed data. Fig. 2 shows the modified system together with relays that perform synchronphasor measurements [6]. The relays receive commands from the SVP to control and protect the power system. The overall system has fewer components than the original scheme, reducing the number of points of failure.

This paper shows how to use synchronphasors in wide-area control applications and substation protection and monitoring. Conventional synchronphasor literature is mistaken in suggesting that these applications are years away. The paper covers the following synchronphasor applications:

- A power system dynamics monitor that calculates angle difference, slip frequency, and acceleration to predict power angle unstable conditions.
- A modal analysis-based SIPS to identify undamped oscillations and take action before the system collapses.
- A distributed busbar differential scheme to protect busbars with as many as 64 terminals.
- A substation processor that identifies measurement errors and filters erroneous measurements before sending these measurements to upper-tier applications.
- Measurement error identification, measurement refinement, and measurement supervision through the use of local and remote synchronphasor measurements.

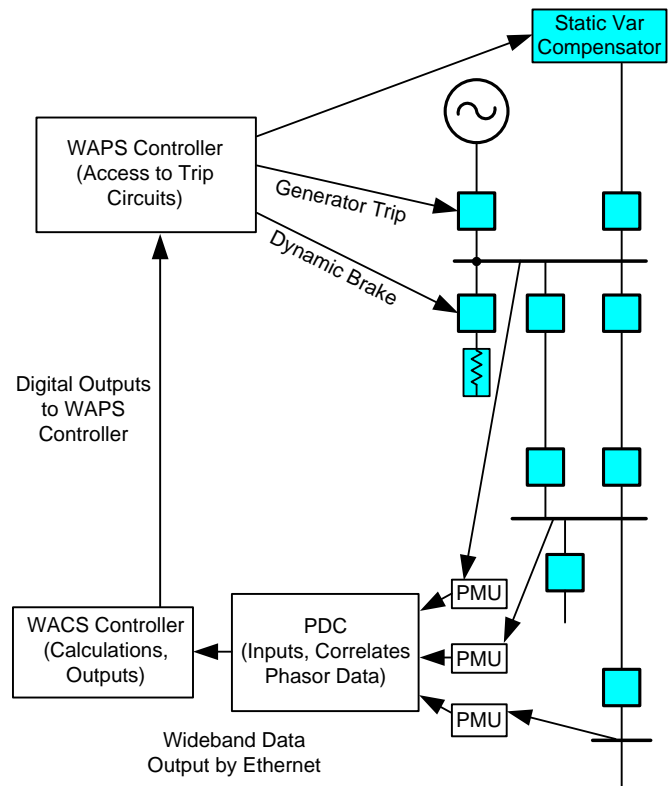


Fig. 1. WACS/WAPS control that uses one PDC and PMUs

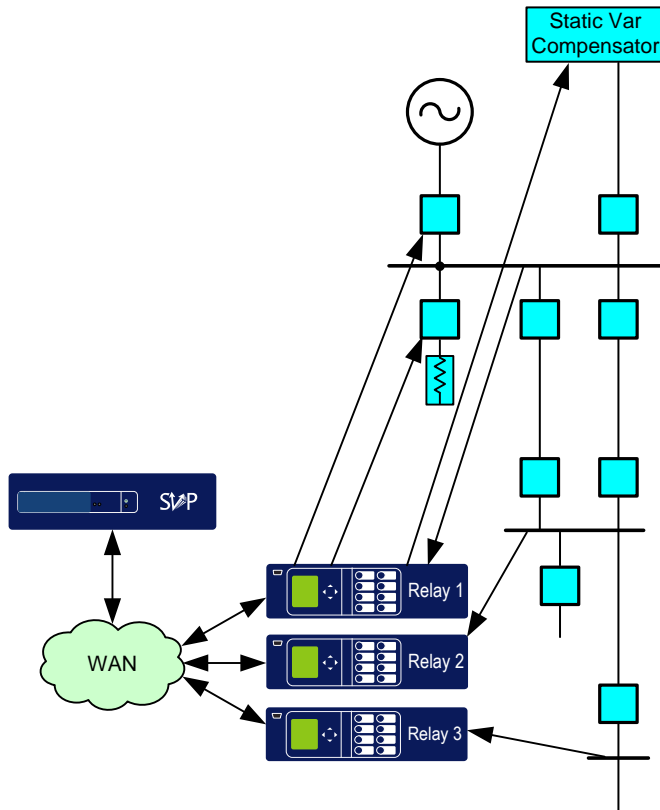


Fig. 2. Integrated SIPS that uses SVP and relays simplifies wide-area applications

II. SVP BASIC FUNCTIONALITY

The SVP, shown in Fig. 3, receives synchrophasors and sends commands for real-time power monitoring, protection, automation, and control. The SVP includes the following components:

- Communications Interface
- Time Alignment, Client, and Server
- Run-Time System (RTS)

A. Communications Interface

The SVP uses serial or Ethernet communications to collect synchrophasor measurements from relays, meters, PMUs, and PDCs and to send commands to relays or I/O devices. The SVP also sends a programmable synchrophasor message to external synchrophasor clients.

B. Time Alignment, Client, and Server (TCS)

The TCS time aligns incoming synchrophasor messages from external servers and transmits the time-aligned data to the RTS and to external synchrophasor clients.

C. Run-Time System

The RTS is a real-time processing engine within the SVP that runs applications using custom logic and predefined function blocks. The RTS includes the following function blocks:

- Power Calculation: calculates the active and reactive power from voltage and current phasors.
- Phase Angle Difference Monitor: calculates the angle difference between two phasor angles and provides angle difference alarms.
- Modal Analysis (MA): calculates the modes of signals available within the RTS.
- Substation State and Topology Processor (SSTP): identifies measurement errors, calculates current unbalance and symmetrical components, and refines voltage and current measurements.
- Commands: The SVP can issue multiple commands to activate remote controls.

D. Programmable Synchrophasor Message

The SVP includes seven synchrophasor message outputs, one of which is programmable and referred to as Local PMCU. Local PMCU outputs synchrophasor messages over Ethernet. The Local PMCU message can include any of the signals available within the RTS for upper-tier applications.

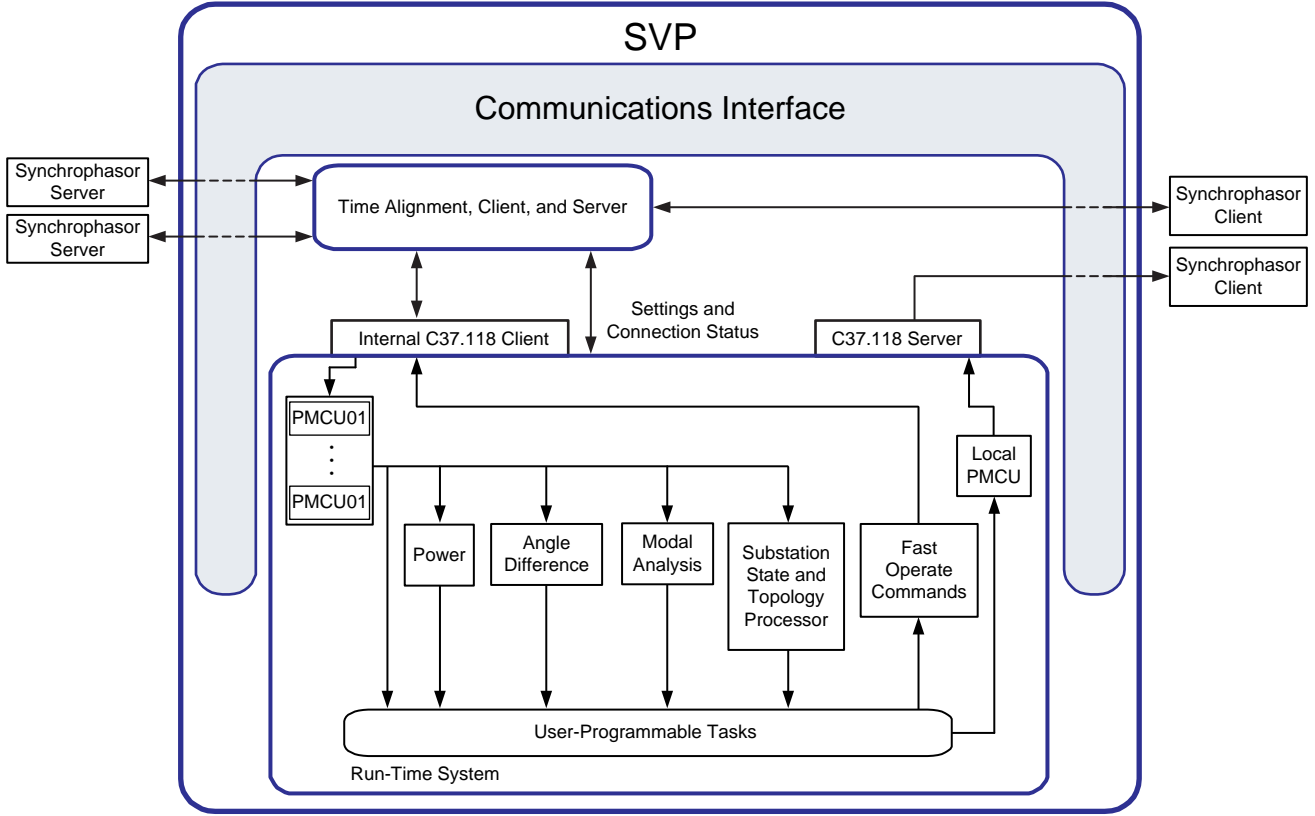


Fig. 3. SVP includes function blocks and programmable logic to activate commands

III. DETECTING POWER SWINGS TO PREVENT SYSTEM DISTURBANCES

This section describes a SIPS that detects power swings and out-of-step conditions and activates remedial actions to prevent power system instability. The SIPS consists of two relays with synchrophasor measurement and control capabilities and one SVP. This SIPS is suitable for two-area power systems.

A. SIPS for Two-Area Power Systems

In a two-area power system, the electrical center is the point that corresponds to half of the total impedance between the two sources [2]. The electrical center of the system can be at a transmission line or at any other part of the system that corresponds to half of the total impedance. The proposed SIPS requires that the system electrical center must be between the relays that acquire the synchrophasor measurements. These relays also include programmable logic capabilities to program outputs and perform remedial actions. Reference [7] describes a SIPS for out-of-step tripping that processes 20 synchrophasor messages per second. Fig. 4 shows an alternative to the SIPS presented in [7] that uses the SVP to collect synchrophasor data from two relays at 60 messages per second. In this approach, the SVP runs the SIPS's Out-Of-Step Tripping (OOST) element and sends remedial action commands to the relays that acquire the synchrophasor measurements.

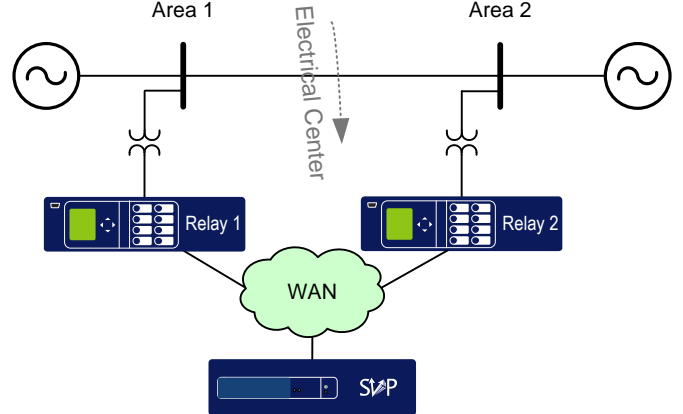


Fig. 4. SIPS suitable for two-area power systems that uses two relays and one SVP for power swing detection

B. Out-of-Step Tripping Element (OOST)

The OOST element that [7] describes uses the positive-sequence voltage synchrophasors that relays acquire at two power system busbars to calculate the angle difference between these voltages δ_k according to (1). The change of δ_k with respect to time defines the slip frequency S_{f_k} (2), and the change of slip frequency with respect to time defines the acceleration A_{f_k} (3) between the two areas. Fig. 5 shows the characteristic of the OOST element [8] that defines the region of power system stable operation. The OOST element uses the slip frequency and acceleration that the SVP calculates to identify the unstable operating conditions. When the operating point is outside the stable region for 150 ms, the

OOST element asserts to indicate this unacceptable operating condition.

$$\delta_k = V_{1_Ang_k}^{Relay 1} - V_{1_Ang_k}^{Relay 2} \quad (1)$$

$$S_{f_k} = \frac{(\delta_k - \delta_{k-1})}{360} MRATE \quad (2)$$

$$A_{f_k} = (S_{f_k} - S_{f_{k-1}}) \cdot MRATE \quad (3)$$

where:

$V_{1_Ang_k}^{Relay 1}$ is the positive-sequence voltage angle of Relay 1 at the k processing interval

$V_{1_Ang_k}^{Relay 2}$ is the positive-sequence voltage angle of Relay 2 at the k processing interval

S_{f_k} is the slip frequency at the k processing interval

A_{f_k} is the acceleration at the k processing interval

$MRATE$ is the synchrophasor message rate

C. Implementation of the OOST SIPS

We use the SVP, shown in Fig 3, to implement the OOST SIPS. In this scheme, the relays send system voltage phasors to the SVP. The SVP uses the RTS to run the logic and algorithms of the OOST element in real time. After time alignment, the positive-sequence voltage phasors that the relays acquire are available to the RTS. The OOST scheme, shown in Fig. 6, includes the following function blocks:

- PMCU01: Relay at Area 1.

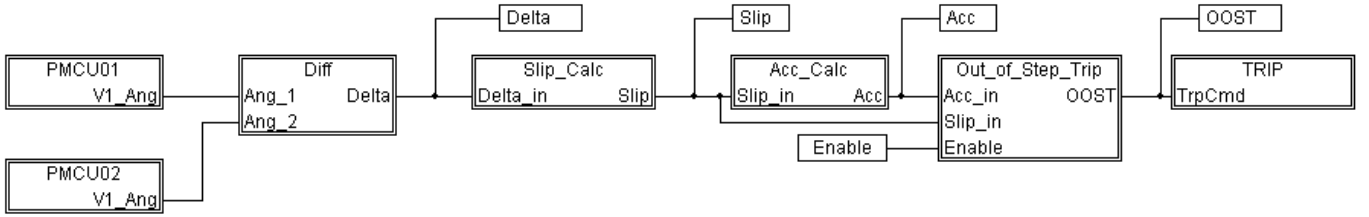


Fig. 6. Implementation of the OOST scheme using the SVP

- PMCU02: Relay at Area 2.
- Diff: Angle difference calculation.
- Slip_Calc: Slip frequency calculation.
- Acc_Calc: Acceleration Calculation.
- Out_of_Step_Trip: Out-of-step tripping algorithm and logic.
- TRIP: Command to send the remedial action.

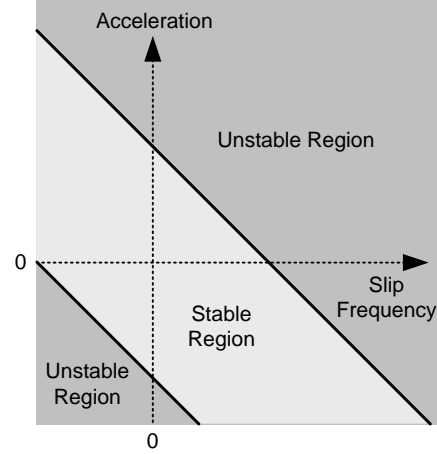


Fig. 5. The out-of-step tripping element uses slip frequency and acceleration information to identify unstable operating conditions

D. Performance of the OOST SIPS

The system in Fig. 7 shows two generators in one area of the power system and a third generator in the other area representing the rest of the power system. In this system, the electrical center is at the transmission line that connects busbars N2 and N3. Fig. 7 also shows the main components of the SIPS and the location of the relays that acquire the synchrophasor measurements. Relay 1 is at the generator busbar N1. Relay 2 is at the system busbar N5. This relay placement ensures that the electrical center of the power system is between the two relays. In this application, the relays send synchrophasor messages over Ethernet to the SVP at 60 messages per second. The SIPS detects unstable power swings and sheds the 396 MVA generator to maintain system stability. We modeled this power system in the Real Time Digital Simulator (RTDS[®]) to analyze the performance of the OOST scheme in real time.

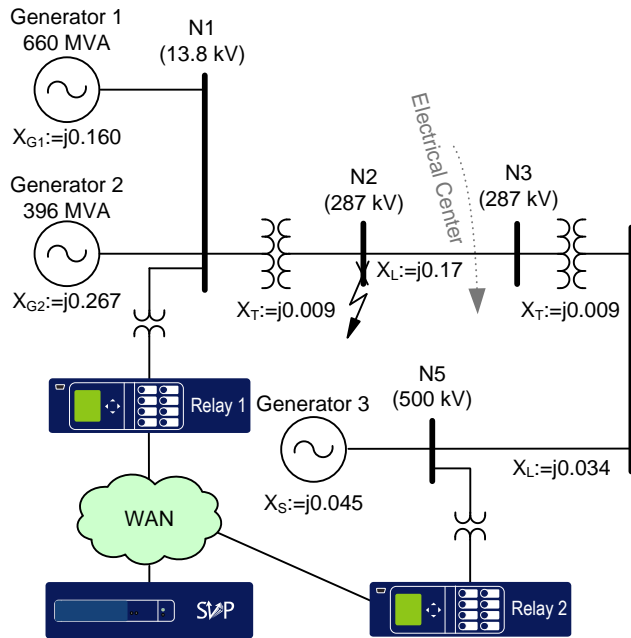


Fig. 7. System model to analyze the performance of the OOST scheme in real time

The power system that we just described experiences a temporary fault at busbar N2 that causes changes in machine angle, speed, and acceleration. We assume that the temporary fault extinguishes automatically. If the fault clearing time exceeds 6.9 cycles, the critical clearing time, the system becomes unstable. Table I describes the three scenarios that we used to analyze the performance of the OOST element.

TABLE I
SCENARIOS TO ANALYZE THE PERFORMANCE OF THE OOST ELEMENT

Scenario 1	Stable operating conditions	The fault clears in 6.0 cycles and the system remains stable.
Scenario 2	Unstable operating conditions without remedial action	The fault clears in 7.0 cycles and the system becomes unstable.
Scenario 3	Unstable operating conditions with remedial action	The fault clears in 7.0 cycles, the operating point remains outside the OOST characteristic longer than 150 ms, the scheme detects this operating condition and trips Generator 2 to maintain system stability.

We use the programmable output message of the SVP together with synchrophasor visualization and archiving software to capture the angle difference, slip frequency and acceleration calculations, and the OOST scheme output in real time.

1) Angle Difference Calculations

Fig. 8, 9, and 10 show the screen captures of the angle difference calculations for the three scenarios. In the first scenario, the system returns to the initial stable operating conditions in approximately 13 seconds. In the second scenario, the angle difference between the two monitored busbars increases beyond 180 degrees after approximately 5.7 seconds, and the system becomes unstable. In the third scenario, the angle difference begins to increase, the OOST scheme detects that the operating point is outside of its characteristic, and the SVP sends the tripping command approximately 0.9 seconds after the fault clears to shed Generator 2 and to maintain system stability. In this case, the final angle difference corresponds to the new operating conditions with Generator 2 out of service.

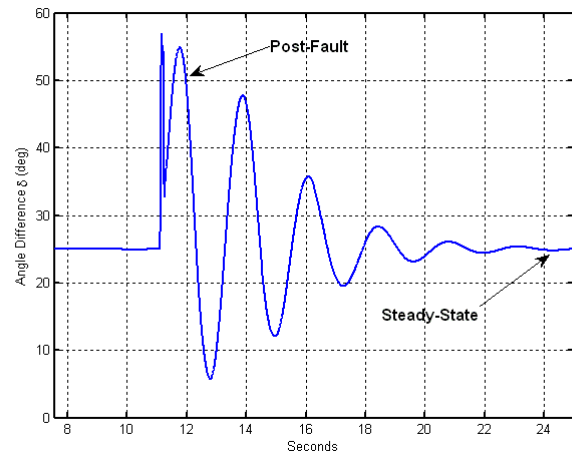


Fig. 8. Angle difference calculations for stable operating conditions

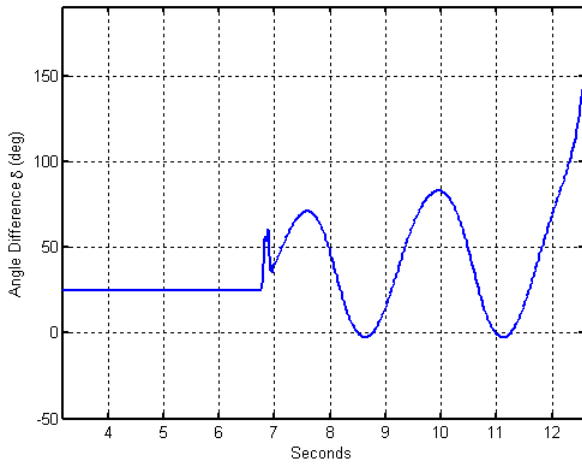


Fig. 9. Angle difference calculations for unstable operating conditions without remedial action

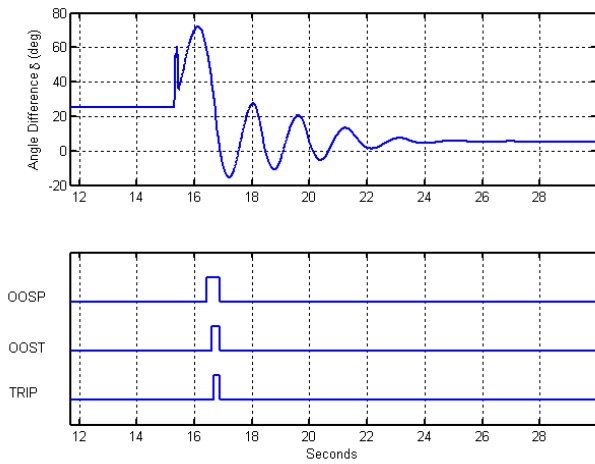


Fig. 10. Angle difference calculations for unstable operating conditions and remedial action to maintain system stability

2) Angle Difference and Slip Frequency Trajectories on the Phase-Slip Frequency Plane

Fig. 11, 12, and 13 show the angle difference and slip frequency trajectories on the phase-slip frequency plane for the three scenarios. Fig. 11 shows the angle difference and slip frequency trajectory after the fault clears for the first scenario. In this case, the operating point returns to the initial stable operating condition. Fig. 12 shows that the operating point increases without restriction after two oscillations for the second scenario. Fig. 13 shows two trajectories for the third scenario: the trajectory before the remedial action and the trajectory after the remedial action. Notice that the angle difference does not increase past 73 degrees, even though the system is about to become unstable.

These trajectories on the phase-slip frequency plane do not allow the scheme to identify the unacceptable operating condition.

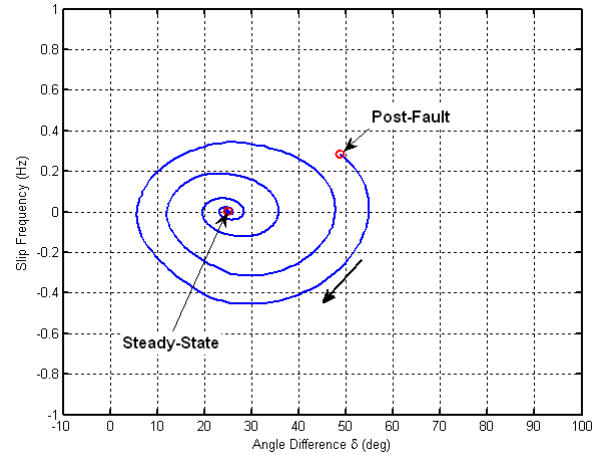


Fig. 11. Angle difference and slip frequency trajectory for stable operating conditions

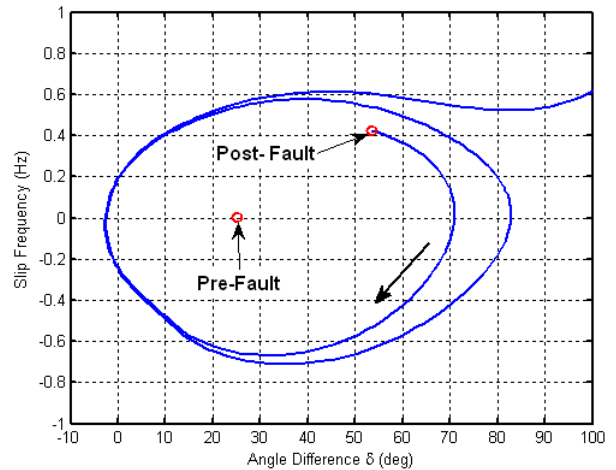


Fig. 12. Angle difference and slip frequency trajectory for unstable operating conditions

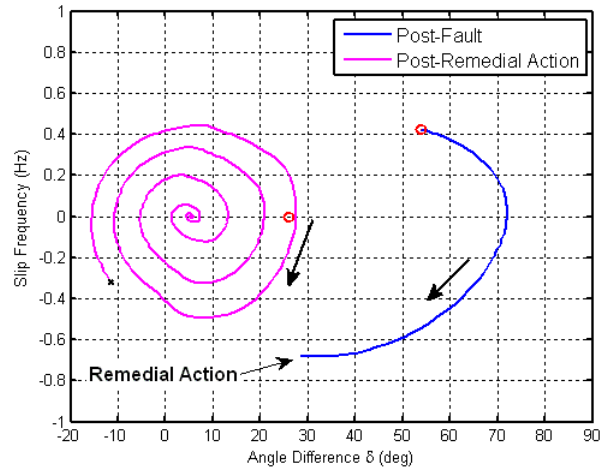


Fig. 13. Angle difference and slip frequency trajectories before and after the 396 MVA generator trips

3) Slip Frequency and Acceleration Trajectories on the Slip Frequency-Acceleration Plane

Fig. 14, 15, and 16 show the slip frequency and acceleration trajectories and the characteristic of the OOST element on the slip frequency-acceleration plane for the three scenarios. In

the first scenario, Fig. 14 shows that the operating point remains inside the stable region of the OOST element characteristic. In the second scenario, Fig. 15 shows that the operating point enters the unstable region in each of the oscillations and then increases without restriction after the second oscillation.

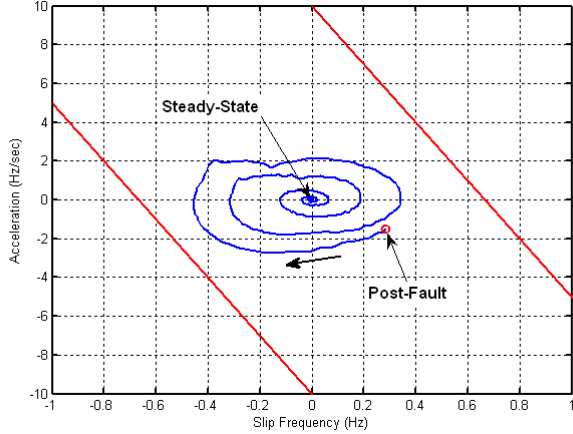


Fig. 14. Slip frequency and acceleration trajectory for stable operating conditions

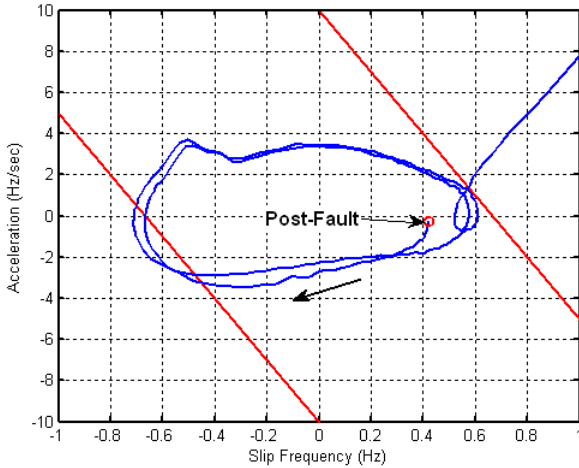


Fig. 15. Slip frequency and acceleration trajectory for unstable operating conditions

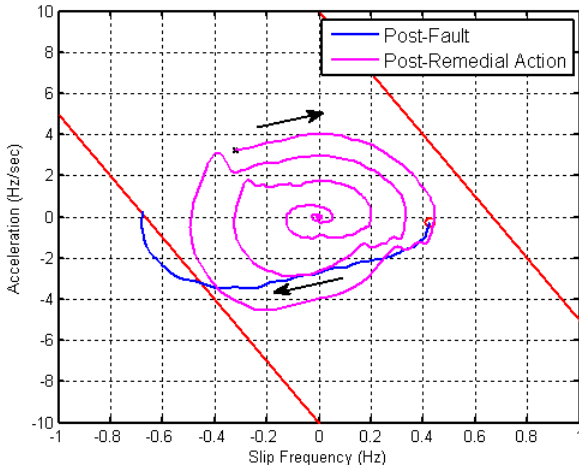


Fig. 16. Slip frequency and acceleration trajectories before and after the 396 MVA generator trips

Fig. 16 shows two trajectories for the third scenario: the trajectory before the remedial action and the trajectory after the remedial action. The operating point remains in the unstable region longer than 150 ms, and the OOST scheme trips Generator 2. After the generator trip, the system remains stable.

IV. POWER SYSTEM INTER-AREA OSCILLATION AND MITIGATION

A. Power System Oscillations and MA

The SVP uses built-in MA function blocks and flexible programming logic equations to detect unstable inter-area oscillations and automatically initiate remedial actions. Power system disturbances, such as line tripping and drop of generation, cause local and inter-area power system oscillations. Usually, local oscillation modes range in frequency from 0.7 to 2.0 Hz [9]. Inter-area oscillation, which refers generally to a group of generators in one area that swing against a group of generators in another area, normally ranges in frequency from 0.1 to 0.8 Hz [9]. The local oscillation involves a few generators within a small portion of a power system and has little impact on an overall power system. Inter-area oscillations constrain the amount of power that can be transferred through some parts of interconnected power grids. Without proper remedial actions, inter-area oscillation can result in power system separations or major blackouts.

The traditional approach to preventing inter-area oscillation involves modal analysis of the results of power system dynamic simulations at the planning stage. The inaccuracy of the power system dynamic model and the number of contingencies and operating conditions available to perform this analysis limit this traditional approach.

We can now use advanced computing and signal-processing technology to detect and mitigate inter-area oscillations in real time. The SVP uses Modified Prony Analysis (MPA) to perform MA. MPA uses the linear combination of multiple exponential oscillation modes to approximate an original signal that a device samples at fixed time intervals. For an array of data samples $x[1], \dots, x[N]$, the MPA estimates $\hat{x}[n]$ according to (4) for $1 \leq n \leq N$ [10].

$$\hat{x}[n] = \sum_{m=1}^M A_m e^{\sigma_m(m-1)T} \cos(2\pi f_m(m-1)T + \phi_m) \quad (4)$$

where:

T is the sample interval in seconds.

A_m is the amplitude of the exponential function.

σ_m is the damping constant in seconds⁻¹.

f_m is the frequency in Hz.

ϕ_m is the initial phase in radians.

M is the number of modes.

The corresponding signal-to-noise-ratio (SNR) calculation in (5) quantifies the quality of the curve fit. MPA is a linear approximation technique, so it will produce a low SNR value if the data sample array contains nonlinear transitions. In power systems, discrete switching events, such as line

tripping, can cause nonlinear transitions. The SNR value normally improves as a switching event leaves the observation window of MA, and the power system settles into pure oscillation mode. A high SNR value (greater than 80 dB, for example) indicates that the analysis result is a good approximation of the original signal.

$$SNR = 10 \log_{10} \left(\frac{\sum_{n=0}^N x[n]^2}{\sum_{n=0}^N (x[n] - \bar{x}[n])^2} \right) \quad (5)$$

B. Inter-Area Oscillation Mode Identification

Power system oscillations are visible in power system quantities such as busbar voltage, angle difference, frequency, active power transfer, and reactive power transfer through transmission lines. MA uses synchrophasor measurements of these power system quantities as an input signal. The MA result includes an array of modes and an SNR value. Each mode is a data structure that includes amplitude A_m , frequency f_m in Hz, damping constant σ_m , damping ratio ζ_m , and initial phase angle φ_m in degrees. Equation (6) calculates the damping ratio from the frequency and the damping constant. A negative damping ratio (positive damping constant σ) indicates that the corresponding mode is an increasing oscillation mode.

$$\zeta_m = \frac{-\sigma_m}{\sqrt{\sigma_m^2 + (2\pi f_m)^2}} \quad (6)$$

The array of calculated oscillation modes includes both local oscillation modes and inter-area oscillation modes. To identify the inter-area oscillation modes from the array of modes, additional logic must process the MA results based on measurements from different areas before control actions can occur. Fig. 17 illustrates the decision-making process based on MA results.

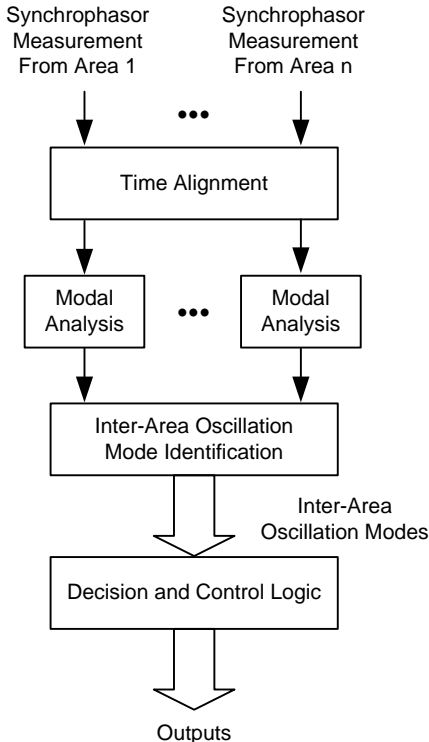


Fig. 17. Remedial action based on modal analysis results

MPA involves numerical approximation, so the calculated mode frequencies from different areas can vary for a common inter-area oscillation mode. Therefore, the process of identifying the common oscillation modes normally uses a frequency deviation threshold. The SVP identifies a common oscillation mode if the difference between the calculated mode frequencies within a group and their mean value is less than a user-specified threshold.

The SVP then feeds the parameters of the common inter-area oscillation mode to the Decision and Control Logic block. This block activates alarm and control output signals. Fig. 18 illustrates an example of the decision and control logic. The SNR must be greater than SNR_{thre} to enable the control signal output. The f_{high} and f_{low} thresholds define the frequency band of the inter-area oscillation mode in which we are interested. The mode frequency f_m must be within this frequency band to activate the control signal output. If the mode amplitude A_m is greater than A_{thre} , the damping ratio ζ_m is less than ζ_{thre} , and the condition persists longer than the damping ratio pickup ($DRPU$), the alarm or control output asserts.

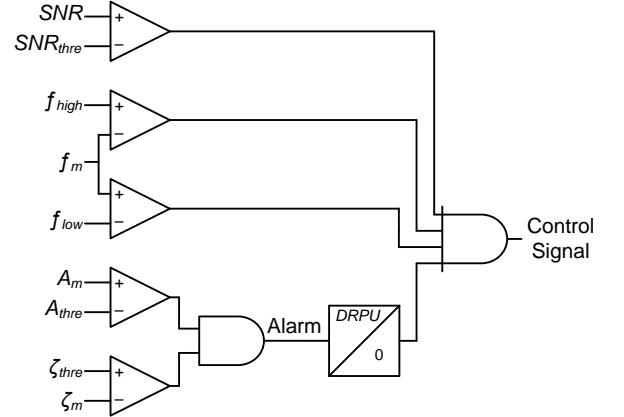


Fig. 18. Oscillation mode-based decision and control logic

C. MA-Based SIPS Example

Fig. 19 shows a two-area power system model that we can use to test scheme performance. Past literature has used this power system model with small variations to illustrate the inter-area oscillation problem [10] [11]. The system parameters we use here are almost identical to [11], except that we modeled the load as a constant load ($V > 0.80$ pu) instead of as a constant impedance to obtain more realistic results. The analytic result shows that the system has three dominant oscillation modes. Each area has a local oscillation mode, and there is one inter-area oscillation mode.

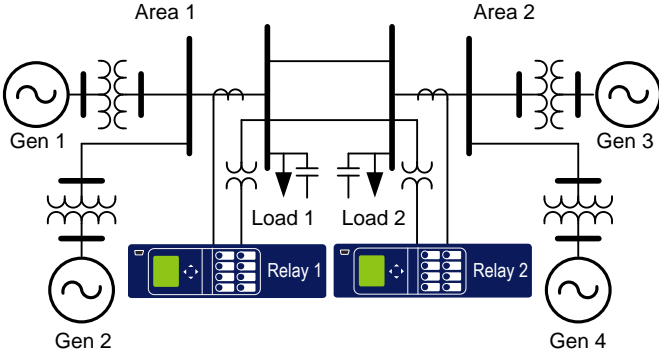


Fig. 19. Two-area power system model with an inter-area oscillation problem

We use an RTDS to simulate power system dynamics. Fig. 20 shows the system to evaluate the scheme. Two relays measure the currents and voltages in real time at both sides of the intertie. The relays send synchrophasor measurements (voltage and current) to the SVP via Ethernet at 30 messages per second in the IEEE C37.118 protocol [12]. The SVP internally aligns the synchrophasor measurements from the relays according to measurement time stamps, calculates the active power measurement of each relay, and then feeds these active power measurements to two independent MA function blocks.

The MA function blocks accommodate various synchrophasor message rates. If the input synchrophasor message rate exceeds the MA data rate setting, the MA function block downsamples the measurement before the modal analysis calculation. The number of data samples for MA equals the data rate multiplied by the observation window. The sliding window setting specifies the number of new samples necessary for each processing interval of MA. In this test case, each MA function block has the settings in Table II. The MA function block calculates the oscillation modes every two seconds (observation window multiplied by the sliding window and then divided by 100).

The SVP feeds results from the two MA function blocks into the logic that identifies inter-area oscillation modes. We set the frequency deviation threshold to 0.01 Hz to identify the common oscillation mode. The control logic, shown in Fig. 18, uses the settings from Table III.

TABLE II
MODAL ANALYSIS SETTING

Estimated # of Modes	Data Rate (Messages/Second)	Observation Window (Seconds)	Sliding Window (Percentage)
15	30	20	10

TABLE III
CONTROL LOGIC SETTING

SNR_{thre} (dB)	f_{low} (Hz)	f_{high} (Hz)	A_{thre} (MW)	ζ_{thre}	$DRPU$ (Seconds)
80	0.1	0.8	0.5	0.0	20

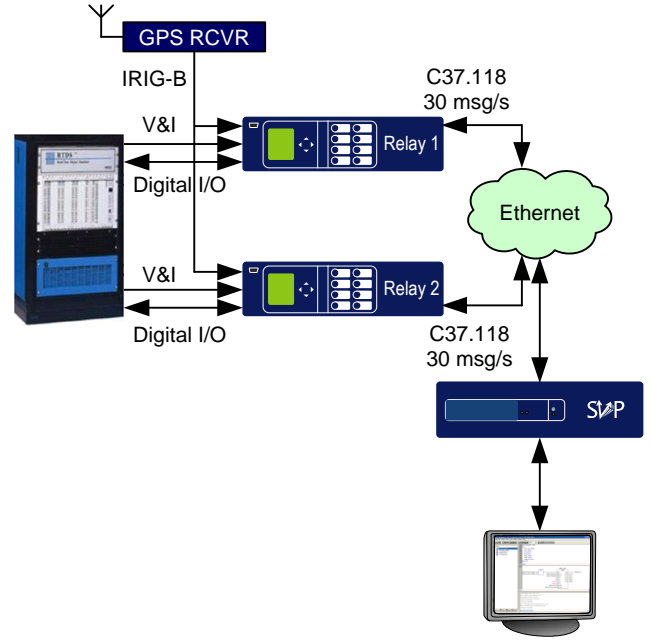


Fig. 20. Power system model in RTDS with synchrophasor data acquisition and SVP

Under steady state, Area 1 exports about 425 MW to Area 2 through the intertie transmission lines. Reducing the Generator 1 active power output reference from 708 MW to 705 MW triggers the increasing oscillation. Without any remedial action, the system will eventually collapse. To maintain power system stability, the SIPS, which we implemented for this test for demonstration purposes, turns on the power system stabilizers of Generator 1 and Generator 3. Fig. 21 shows the inter-area active power transfer during the event. The SVP detects the growing inter-area oscillation mode and asserts an alarm signal approximately 13 seconds after the change of generation output. Table IV lists information about the inter-area oscillation mode as well as the SNR 13 seconds after the change of generation output. The table lists the single inter-area oscillation mode that the modal identification logic identified. This mode has a frequency of about 0.65 Hz.

Twenty seconds after the scheme asserts the alarm signal, the SVP automatically sends a remedial action command via the relays to the RTDS to turn on the power system stabilizers. With the stabilizers in place, the system returns to stable operating conditions approximately 20 seconds after the remedial action.

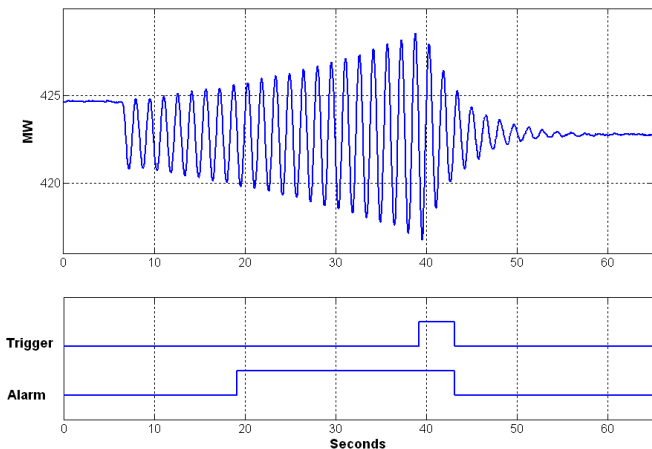


Fig. 21. Inter-area active power transfer and decision logic outputs

TABLE IV
IDENTIFIED INTER-AREA OSCILLATION MODE

	MA1 (P Area 1)	MA2 (P Area 2)
SNR (dB)	124.2	125.6
Mode_1_Amp (MW)	0.657	0.585
Mode_1_Freq (Hz)	0.650	0.649
Mode_1_Damp_Ratio	-1.35%	-1.31%

Fig. 22 shows the damping constant of the inter-area oscillation mode that the SVP identified during the event. Because the sliding window setting is 10 percent of the 20-second observation window, the result updates every two seconds. The damping constant increases to 4 percent, which indicates that the oscillation is increasing and unstable, before the SVP switches on the stabilizers. After the stabilizers are in service, the damping constant decreases from 4 percent to negative damping constants. This negative sign indicates that the oscillation is decaying and that the system has regained stability.

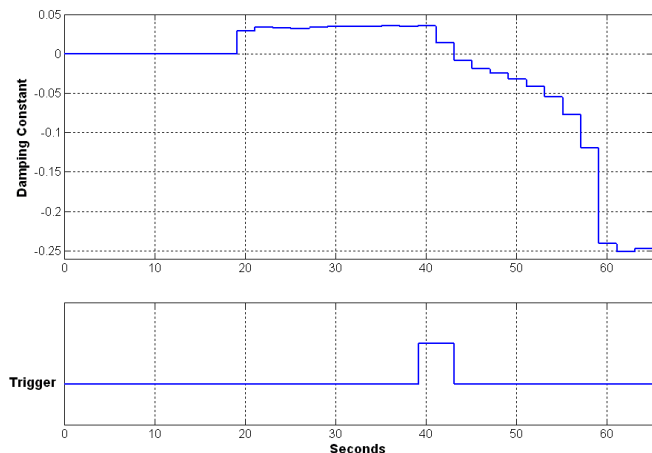


Fig. 22. Inter-area oscillation mode damping constant

V. DISTRIBUTED BUSBAR DIFFERENTIAL PROTECTION

This section describes a backup Busbar Differential Protection Scheme (BDPS) that uses synchrophasors and is suitable for as many as 64 terminals. This scheme uses the Topology Processor available within the SVP to adapt the differential element to different busbar configurations and operating conditions. The scheme consists of one SVP and relays with synchrophasor measurement and control capabilities that measure the currents of all the busbar terminals and send trip commands to the terminal breakers, as Fig. 23 illustrates.

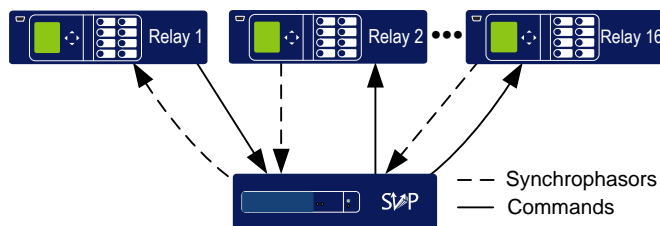


Fig. 23. Distributed busbar differential protection scheme for as many as 64 terminals uses relays at terminal locations and one SVP

The SVP connects to 16 relays with synchrophasor measurement and control capabilities. Each relay can monitor as many as four terminals. The BDPS performs the following tasks:

- Processing the busbar topology information to determine the appropriate protection zones.
- Detecting busbar faults using current phasors and protection zone information.
- Transmitting trip signals to the appropriate relays to clear the busbar fault.

A. Protection Zone Selection

The BDPS uses the topology and current processors built into the Substation State and Topology Processor (SSTP) module to determine the protection zones, as Fig. 24 illustrates. The topology processor generates lists of branches within each protection zone. The SSTP requires the busbar topology information, the status of breakers and disconnects, the current transformer polarities, and the terminal current measurements.

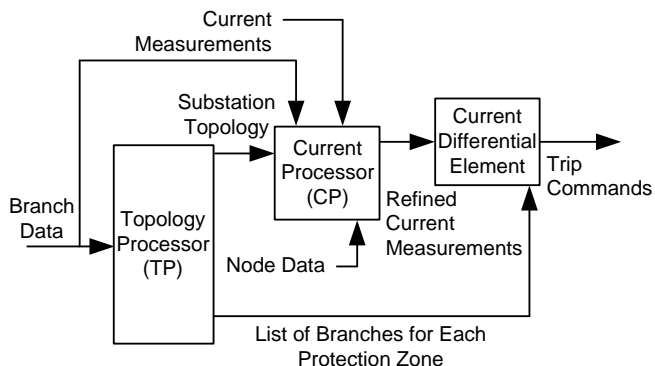


Fig. 24. The distributed busbar protection scheme uses the topology and current processors to determine the busbar protection zones

B. Current Differential Element

The current differential element, shown in Fig. 25, uses the refined currents from the Current Processor (CP) and the list of branches for each protection zone to detect busbar faults. The SVP accommodates as many as 300 differential elements. Using the current phasors I_{01}, \dots, I_{64} , the differential element calculates the restraint quantity I_{RT} and the operating quantity I_{OP} according to (7) and (8). The differential element characteristic consists of two slopes: $SLP1$ and $SLP2$. $SLP1$ is effective for internal faults, and $SLP2$ is effective for external faults. This slope's adaptability adds security to the filtered differential element during external fault conditions. The function that generates the differential element characteristic has two output bits. The first bit $FDIF$ indicates that I_{OP} is greater than $I_{RT} \cdot SLPn$. The second bit $87O$ indicates that I_{OP} is greater than the differential element threshold $O87P$. Assertion of these two bits indicates that the operating point is in the tripping region of the differential element characteristic.

$$I_{RT} = |I_{01}| + |I_{02}| + \dots + |I_{64}| \quad (7)$$

$$I_{OP} = |I_{01} + I_{02} + \dots + I_{64}| \quad (8)$$

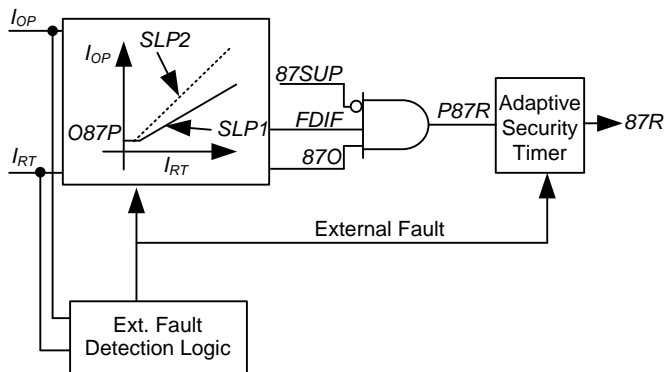


Fig. 25 Current differential element characteristic, external fault detection logic, and $87R$ output logic

The External Fault Detection Logic monitors the change of I_{RT} with respect to I_{OP} to detect external faults. If there is a change of I_{RT} and no change in I_{OP} , the logic declares an external fault condition [13], the differential element slope changes to $SLP2$, and the security timer increases its pickup time to increase the security of the differential element. This logic requires that current transformers (CTs) reproduce the primary current without saturation for at least one cycle.

If bits $FDIF$ and $87O$ are asserted, and there is no CT trouble ($87SUP$ is not asserted), the $P87R$ bit asserts to drive the Adaptive Security Timer. If the $P87R$ bit asserts for longer than the pickup time of the Adaptive Security Timer, $87R$ asserts to indicate a fault in the differential zone.

C. Application Example of the Busbar Differential Protection

To measure the BDPS total fault clearing time for internal faults and security for external faults, we modeled the internal F1 and external F2 faults in a substation with double busbar and transfer busbar, as Fig. 26 illustrates.

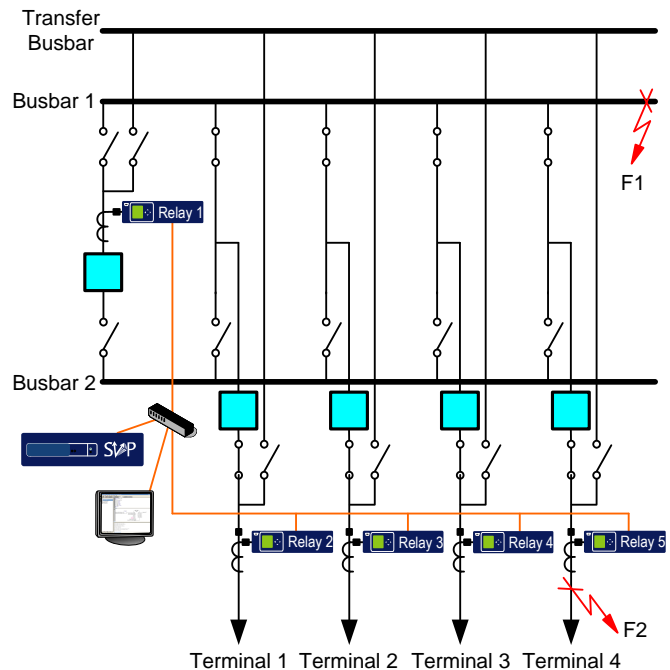


Fig. 26. Distributed busbar protection for double busbar and transfer busbar with multiple terminals

In our test setup, the RTDS generates the current signals, emulates the behavior of CTs, and tracks the status of breakers and disconnects. The simulator feeds the currents from the monitored terminals through a low-voltage level interface. The simulator control outputs are connected to the relay inputs to provide the status of breakers and disconnects. Fig. 27 shows the interconnections of the power system simulator, relays, and SVP and the data exchange among these devices. The relays calculate synchrophasors from the current signals, combine these phasor quantities with the status of breakers and disconnects to create the corresponding synchrophasor message, and send this message to the SVP.

When the SVP detects a busbar fault, it sends a GOOSE message to the tripping relay. The relay then sends trip signals to corresponding breakers, within the simulator, to clear the fault. Before clearing the fault, the simulator introduces a 33 ms delay to emulate the operating time of the breaker.

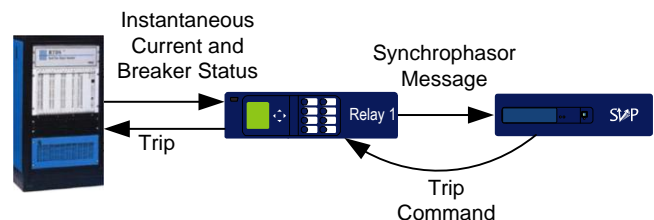


Fig. 27. Interconnection of the power system simulator, relays, and SVP showing exchange among devices

1) Performance for Internal Faults

The oscillogram in Fig. 28 shows the currents for each of the busbar terminals for the internal fault F1 (see Fig. 26). Before the fault, Terminals 1, 2, and 3 feed current to a load that is connected to Terminal 4. A voltage drop at Busbar 1 causes a drop in the load current when the fault is present. Forty-five ms after the inception of the fault, the relays receive

a trip command from the SVP. This operating time makes the BDPS suitable for distribution applications. The breakers of Terminals 1, 2, 3, and 4 clear the fault two cycles after they receive the trip command. In this case, the total operating time is less than 85 ms.

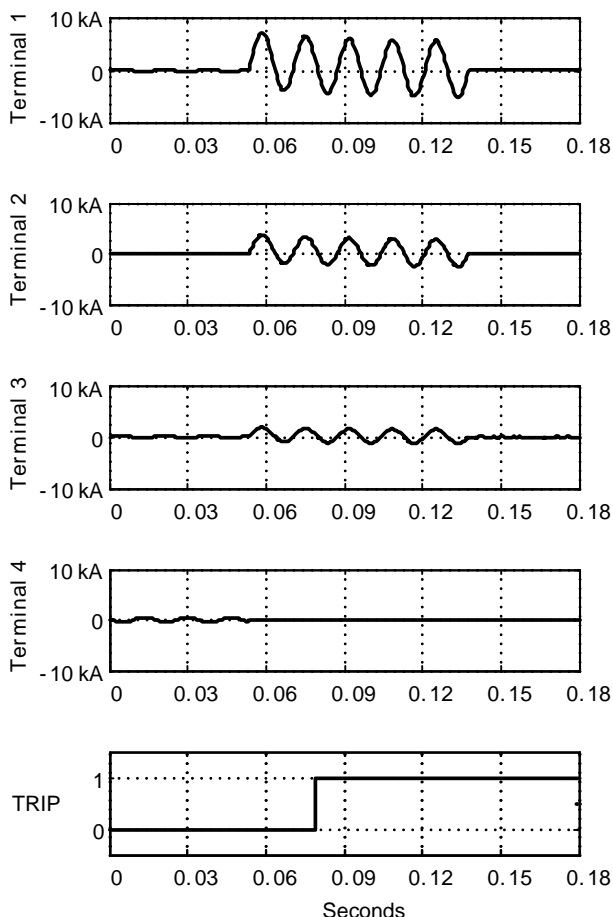


Fig. 28. The distributed busbar differential protection system clears an internal busbar fault in less than 85 ms

2) Performance for External Faults

The oscillogram in Fig. 29 shows the currents of Terminals 1, 2, 3, and 4 for fault F2 (see Fig. 26). Fault F2 is on Terminal 4 outside of the differential protection zone. The fault current causes the CT at Terminal 4 to saturate, but it does not cause misoperation of the differential scheme. Note that the SVP does not activate the trip command to the relays.

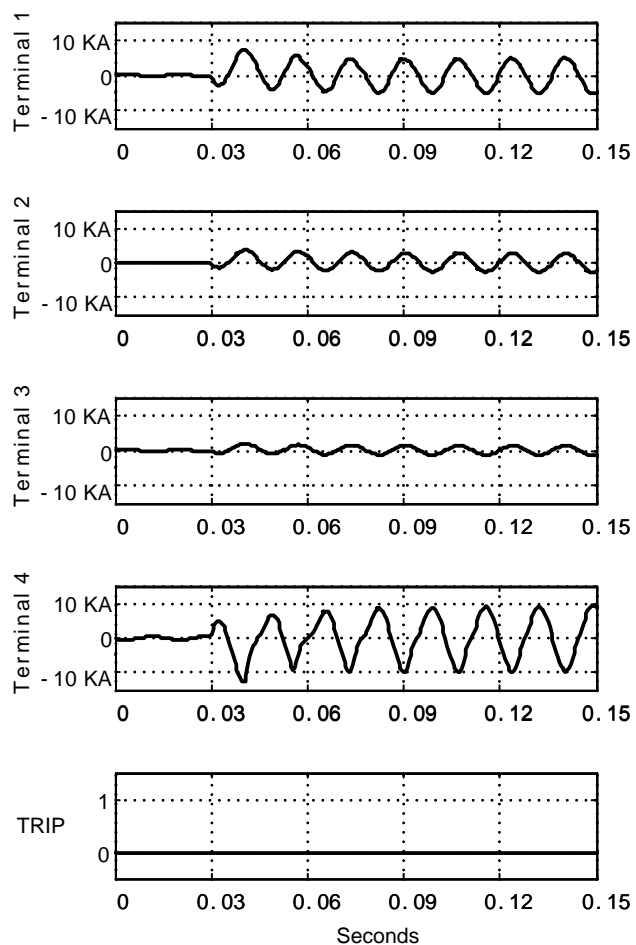


Fig. 29. The distributed busbar differential protection system does not operate for an external fault with current transformer saturation

VI. MEASUREMENT ERROR IDENTIFICATION AND MEASUREMENT SUPERVISION

The CP automatically verifies Kirchhoff's Current Law (KCL) and refines current measurements. The SVP can also use synchrophasors from adjacent substations to supervise voltage measurement from remote locations.

A. KCL Verification

The current processor computes the sum of currents (KCL) reaching every current node group on a per-phase basis. When all currents reaching a group of nodes are available for KCL check, the CP compares the sum of the currents against the user-supplied KCL threshold, KCL_{thre} . If the magnitude of the sum of the measurements is less than the user-supplied KCL threshold, the CP sets the KCL_OK flag for all the involved phase currents and refines the measurement values. Otherwise, at least one of the measurements is bad and no refinement occurs. Consider Fig. 30, in which A_1 , A_2 , and A_3 are the A-phase current measurements on the three branches reaching Node 1.

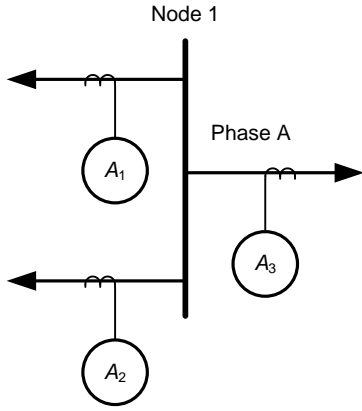


Fig. 30. Current measurements for current measurement refinement

Equation (9) presents the sum condition for our example. To refine these measurements, we find \hat{I}_1 , \hat{I}_2 , and \hat{I}_3 by minimizing the overall error, ε , that (10) defines. The \hat{I}_1 , \hat{I}_2 , and \hat{I}_3 currents are the refined current measurements.

$$\left| \sum_{i=1}^3 A_i \right| > KCL_thre \quad (9)$$

$$\varepsilon = \left| \sum_{i=1}^3 \hat{I}_i \right| + |\hat{I}_1 - A_1| + |\hat{I}_2 - A_2| + |\hat{I}_3 - A_3| \quad (10)$$

B. Current Measurement Refinement

To obtain the solution of the minimization problem in (10), we rewrite (10) in matrix form. Then, the problem becomes finding values for \hat{I}_1 , \hat{I}_2 , and \hat{I}_3 that minimize (11).

$$\left\| \begin{bmatrix} 1 & 1 & 1 \\ 1 & 0 & 0 \\ 0 & 1 & 0 \\ 0 & 0 & 1 \end{bmatrix} \begin{bmatrix} \hat{I}_1 \\ \hat{I}_2 \\ \hat{I}_3 \end{bmatrix} - \begin{bmatrix} 0 \\ A_1 \\ A_2 \\ A_3 \end{bmatrix} \right\| \quad (11)$$

Using the pseudo-inverse [14] [15] of the matrix, we can derive the current estimates for \hat{I}_1 , \hat{I}_2 , and \hat{I}_3 from (12).

$$\begin{bmatrix} \hat{I}_1 \\ \hat{I}_2 \\ \hat{I}_3 \end{bmatrix} = \begin{bmatrix} 3/4 & -1/4 & -1/4 \\ -1/4 & 3/4 & -1/4 \\ -1/4 & -1/4 & 3/4 \end{bmatrix} \begin{bmatrix} A_1 \\ A_2 \\ A_3 \end{bmatrix} \quad (12)$$

Equation (13) is an alternative way, in algebraic form, to derive the current estimates.

$$\hat{I}_i = A_i - \sum_{j=1}^n \frac{A_j}{n+1} \quad (13)$$

where:

n is the number of currents reaching the node.

A_i is the current measurement of branch i .

\hat{I}_i is the current measurement estimate of branch i .

The current processor uses (13) for all the currents reaching each node. For example, if the measured currents are as follows:

$$\begin{aligned} A_1 &= 0.74973 - j0.84335 \\ A_2 &= 0.75851 - j0.49580 \\ A_3 &= -1.50736 + j1.33895 \end{aligned}$$

then, the refined measurements are as follows:

$$\begin{aligned} \hat{I}_1 &= 0.74943 - j0.84328 \\ \hat{I}_2 &= 0.75822 - j0.49574 \\ \hat{I}_3 &= -1.50765 + j1.33902 \end{aligned}$$

C. Remote Measurement Supervision

The SVP can gather and process data from different substations, so it can supervise local and remote redundant measurements. The SVP uses the local busbar voltage, the impedance of the transmission line between the local and remote busbars, and the current on the transmission line between these busbars to supervise the remote voltage measurement. Fig. 31 shows the major components of this voltage supervision scheme. Relay 1 and Relay 2 gather data from the local and remote substations. Relay 1 sends the local voltage V_{L_Meas} and the current on the transmission line I_{L_Meas} to the SVP. Relay 2 sends the remote voltage V_{R_Meas} to the SVP. The SVP also requires transmission line parameters to calculate the remote voltage. We use the pi model, shown in Fig. 32, to represent the transmission line.

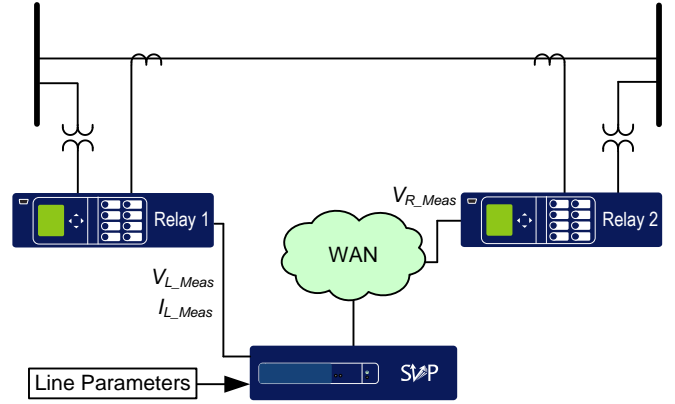


Fig. 31. Scheme to supervise remote voltage measurements

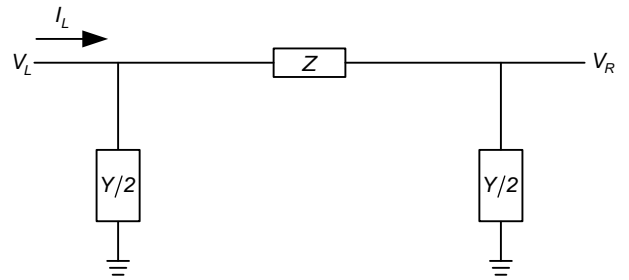


Fig. 32. Model of a transmission line

We use (14) to express the remote voltage in terms of the local voltage and current.

$$V_R = V_L - Z \left(I_L - \frac{Y}{2} \cdot V_L \right) \quad (14)$$

where:

Z is the impedance of the transmission line.

Y is the admittance of the transmission line.

We substitute the voltage and current measurements (V_{L_Meas} and I_{L_Meas}) to calculate the voltage at the remote end according to (15).

$$\hat{V}_R = V_{L_Meas} - Z \left(I_{L_Meas} - \frac{Y}{2} V_{L_Meas} \right) \quad (15)$$

The SVP monitors the error quantity that (16) defines to determine the measurement errors.

$$\varepsilon_V = \left| \hat{V}_R - V_{R,Meas} \right| \quad (16)$$

We implement (16) in SVP programmable logic to monitor the measurement error. This logic sets the remote voltage alarm if the error exceeds a user-specified threshold.

VII. CONCLUSIONS

The Synchrophasor Vector Processor (SVP) acquires synchrophasor measurements from relays located at different geographical areas to run synchrophasor applications. Applications of the SVP include closed loop control schemes for detecting and mitigating unstable power swing conditions, unstable power inter-area oscillations, and remote measurement supervision.

Real-time digital simulations of the power swing detection scheme show the benefit of using the acceleration between two power system areas to identify out-of-step operating conditions before the system becomes unstable.

The SVP provides configurable modal analysis (MA) function blocks. Users then develop decision and control logic based on MA results. Test results demonstrate that the scheme can detect unstable inter-area oscillations early and initiate automatic remedial actions to mitigate unstable oscillations.

In substation applications, the SVP and relays with synchrophasor capabilities can provide distributed busbar differential protection to protect complex busbar arrangements with as many as 64 feeders. This differential protection detects busbar faults in less than three cycles.

VIII. REFERENCES

- [1] E. O. Schweitzer, III and D. E. Whitehead, "Real Time Power System Control Using Synchrophasors," in *2007 34th Annual Western Protective Relay Conference Proceedings*.
- [2] A. Guzmán, D. Tziouvaras, E. O. Schweitzer III, and K. E. Martin, "Local and Wide-Area Network Protection Systems Improve Power System Reliability," in *2004 31st Annual Western Protective Relay Conference Proceedings*.
- [3] *Communication Networks and Systems in Substations*, IEC Standard 61850.
- [4] D. Woodward, "SEL-421 Relay Fast Messages," SEL Application Guide (AG2002-14), 2002. Available: <http://www.selinc.com/aglist.htm>.
- [5] K. C. Behrendt, "Relay-to-Relay Digital Logic Communication for Line Protection, Monitoring, and Control," in *1997 51st Annual Georgia Tech Protective Relaying Conference Proceedings*.
- [6] G. Benmouyal, E. O. Schweitzer, III, and A. Guzmán, "Synchronized Phasor Measurement in Protective Relays for Protection, Control, and Analysis of Electric Power Systems," in *2002 29th Annual Western Protective Relay Conference Proceedings*.
- [7] A. Guzmán, V. Mynam, and G. Zweigle, "Backup Transmission Line Protection for Ground Faults and Power Swing Detection Using Synchrophasors," in *2007 34th Annual Western Protective Relay Conference Proceedings*.
- [8] E. O. Schweitzer, III, T. T. Newton, and R. A. Baker, "Power Swing Relay Also Records Disturbances," in *1986 13th Annual Western Protective Relay Conference Proceedings*.
- [9] M. Klein, G. J. Rogers, and P. Kundur, "A Fundamental Study of Inter-area Oscillations in Power Systems", *IEEE Trans. Power Systems*, vol. 6, no. 3, August 1991, pp. 914–921.
- [10] S. L. Marple, *Digital Spectral Analysis with Applications*, Englewood Cliffs, New Jersey: Prentice-Hall Inc., 1987, p. 304.

- [11] "Performance of Three PSS for Inter-area Oscillations (phasor)," *MATLAB SimPowerSystems Demos*, MathWorks™ [Online]. Available: <http://www.mathworks.com>
- [12] *IEEE Synchrophasors for Power Systems*, IEEE Standard C37.118-2005.
- [13] A. Guzman, C. Labuschagne, and B. Qin "Reliable Busbar and Breaker Failure Protection With Advanced Zone Selection," in *2004 31st Annual Western Protective Relay Conference Proceedings*.
- [14] E. H. Moore, "On the reciprocal of the general algebraic matrix", *Bulletin of the American Mathematical Society*, vol. 26, pp. 394–395, 1920.
- [15] R. Penrose, "A generalized inverse for matrices," *Proceedings of the Cambridge Philosophical Society*, vol. 51, pp. 406–413, 1955.

IX. BIOGRAPHIES

Edmund O. Schweitzer, III is recognized as a pioneer in digital protection and holds the grade of Fellow of the IEEE, a title bestowed on less than one percent of IEEE members. In 2002 he was elected a member of the National Academy of Engineering. He is the recipient of the Graduate Alumni Achievement Award from Washington State University and the Purdue University Outstanding Electrical and Computer Engineer Award. In September 2005, he was awarded an honorary doctorate from Universidad Autónoma de Nuevo León in Monterrey, Mexico, for his contribution to the development of electric power systems worldwide. He has written dozens of technical papers in the areas of digital relay design and reliability and holds more than 30 patents pertaining to electric power system protection, metering, monitoring, and control. Dr. Schweitzer received his Bachelor's degree and his Master's in electrical engineering from Purdue University, and his Ph.D. degree from Washington State University. He served on the electrical engineering faculties of Ohio University and Washington State University, and in 1982 he founded Schweitzer Engineering Laboratories, Inc. to develop and manufacture digital protective relays and related products and services. Today SEL is an employee-owned company, which serves the electric power industry worldwide, and is certified to the international quality standard ISO 9001. SEL equipment is in service at voltages from 5 kV through 500 kV, to protect feeders, motors, transformers, capacitor banks, transmission lines, and other power apparatus.

David E. Whitehead, P.E. is the vice president of Research and Development at Schweitzer Engineering Laboratories, Inc. Prior to joining SEL, he worked for General Dynamics, Electric Boat Division as a combat systems engineer. He received his B.S.E.E. from Washington State University in 1989, his M.S.E.E. from Rensselaer Polytechnic Institute in 1994, and is pursuing his Ph.D. at the University of Idaho. He is a registered professional engineer in Washington State and Senior Member of the IEEE. Mr. Whitehead holds seven patents with several others pending. He has worked at SEL since 1994 and has been responsible for the design of advanced hardware, embedded firmware, and PC software as a hardware engineer, research engineer, and chief engineer/assistant director.

Armando Guzmán received his B.S.E.E. with honors from Guadalajara Autonomous University (UAG), Mexico, in 1979. He received a diploma in fiber-optics engineering from Monterrey Institute of Technology and Advanced Studies (ITESM), Mexico, in 1990, and his M.S.E.E. from University of Idaho, USA, in 2002. He served as regional supervisor of the Protection Department in the Western Transmission Region of the Federal Electricity Commission (the electrical utility company of Mexico) in Guadalajara, Mexico for 13 years. He lectured at UAG and University of Idaho in power system protection and power system stability. Since 1993 he has been with Schweitzer Engineering Laboratories, Inc. in Pullman, Washington, where he is presently Research Engineering Manager. He holds several patents in power system protection and metering. He is a senior member of IEEE.

Yanfeng Gong received his B.S.E.E. from Wuhan University, Wuhan, China in 1998, his M.S.E.E. from Michigan Technological University, Houghton, MI, in 2002 and his Ph.D. in Electrical Engineering from Mississippi State University in 2005. He is currently working with Schweitzer Engineering Laboratories, Inc. as a research engineer in Pullman, Washington. He is a member of IEEE.

Marcos Donolo received his Bachelor's degree in electrical engineering from Universidad Nacional de Rio Cuarto, Argentina in 2000, his Master's degree in electrical engineering from the Virginia Polytechnic Institute and State University in 2002, his Master's in mathematics from the Virginia Polytechnic Institute and State University in 2005, and his Ph.D. in electrical engineering from the Virginia Polytechnic Institute and State University in 2006. Since 2006, he has worked with Schweitzer Engineering Laboratories, Inc., where he is presently a Research Engineer. He is a member of IEEE.